Q-switched Er-doped fiber laser with low pumping threshold using graphene saturable absorber

R. Z. R. R. Rosdin[1], F. Ahmad[1,2], N. M. Ali[1], S. W. Harun[1], and H. Arof[1*]

[1]Department of Electrical Engineering, Faculty of Engineering, University of Malaya, Kuala Lumpur 50603, Malaysia

[2]Department of Electrical Engineering, Universiti Teknologi Malaysia, Kuala Lumpur 54100, Malaysia

[*]Corresponding author: ahamzah@um.edu.my

Received April 29, 2014; accepted June 11, 2014; posted online August 23, 2014

We propose a Q-switched Er-doped fiber laser (EDFL) with a threshold pumping power as low as 7.4 mW, and demonstrate using graphene polyvinyl alcohol (PVA) thin film as a passive saturable absorber (SA). The SA is fabricated from graphene flakes, which is synthesized by electrochemical exfoliation of graphite at room temperature in 1% sodium dodecyl sulfate aqueous solution. The flakes are mixed with PVA solution to produce a thin film, which is then sandwiched between two ferrules to form a SA and integrated in the EDFL ring cavity to generate a stable Q-switched pulse train. The pulse train operates at 1560 nm with a threshold pump power of 7.4 mW. At maximum 1480 nm pump power of 33.0 mW, the EDFL generates an optical pulse train with a repetition rate of 27.0 kHz and pulse width of 3.56 μs. The maximum pulse energy of 39.4 nJ is obtained at a pump power of 14.9 mW. This laser can be used as a simple and low-cost light source for metrology, environmental sensing, and biomedical diagnostics.

OCIS codes: 060.3510, 320.7090, 060.2410.

doi: 10.3788/COL201412.091404.

Among the motives of developing Q-switched fiber lasers is to provide an alternative to the bulk pulsed solid-state lasers for many applications that require laser sources operating in the nanosecond to microsecond range such as range finding, remote sensing, industrial processing, and medicine[1–4]. They can be achieved by numerous schemes based on active and passive approaches. Passively Q-switched fiber lasers are normally realized by inserting a saturable absorber (SA) into the cavity. They feature a more compact geometry and simpler setup than active ones, which require additional switching electronics such as acousto-optic modulator[5]. Doped bulk crystals[6], semiconductor SA mirrors (SESAMs)[7], and carbon nanotubes (CNTs)[8,9] are commonly used SAs in passive Q-switching. However, doped crystals that are mostly used in solid-state laser as SAs in fiber laser require extra elements (mirrors and lenses) to focus the fiber output into the crystal. Therefore their operating range is limited in a small bandwidth. SESAMs also have limited operating bandwidth, typically few tens of nanometers[7], which are not suitable for broadband tunable pulse generation. Compared with SESAMs, CNTs can be regarded as the broadband SAs, operated on Yb-doped[10], Er-doped[11], and Tm-doped fiber lasers[12]. However, its operation wavelength is related to diameter and chirality of the CNTs.

Recently, graphene, a single layer of carbon in a hexagonal lattice, has been intensively researched due to its wonderful optical properties[13,14]. In laser photonics, graphene SA has been widely used as a broadband SA to passively Q-switch or mode-lock fiber laser or solid-state laser, at different laser wavelengths ranging from 1 to 2 μm[15,16]. Till date, many works have been reported on the integrating graphene SA into fiber laser system for ultrashort-pulse generation. For instance, mode-locked Er-doped fiber laser (EDFL) with stable soliton-like pulse output was achieved using a graphene from a chemical vapor deposition process[17]. We demonstrate a Q-switched EDFL with low pumping threshold using a graphene embedded into polyvinyl alcohol (PVA) composite. The SA is in the form of composite film, which is fabricated from graphene flakes obtained from electrochemical exfoliation. The SA is integrated in the EDFL by sandwiching the graphene thin film between two fiber connectors to achieve a stable pulse train operating at 1560 nm with a threshold pump power of 7.4 mW. The performance of the EDFL is also investigated with a graphene poly ethylene oxide (PEO) SA for comparison.

Here the key part is the fabrication of SA film based on graphene sheet in PVA host. The PVA is a water-soluble synthetic polymer with monomer formula C_2H_4O, which has excellent film forming, emulsifying, and adhesive properties. It also has high-tensile strength, flexibility, high oxygen, and aroma barrier, although these properties are dependent on humidity. Graphene flakes were produced using electrochemical exfoliation process. In this process, a constant voltage difference of 20 V was applied to two electrodes (graphite rods), which are placed 1 cm apart in an electrolysis cell filled with electrolyte (1% sodium dodecyl

sulfate (SDS) in deionized water). Hydroxyl and oxygen radicals were generated due to electrolysis of the water at the electrode during the electrochemical process. Then oxygen radicals started to corrode the graphite anode. This was followed by the intercalation of anionic surfactant and finally graphene sheets were created in the solution. In this work, black sediments (graphene) started to peel off from the anode after several minutes. The exfoliation process was continued for 2 h to obtain a stable graphene suspension in the SDS solution. The stable graphene suspension was centrifuged at 3000 rpm for 30 min to remove large agglomerates. Then supernatant portion of the suspension was decanted. The next step was to prepare a PVA solution by dissolving 1 g of PVA in 120 mL distilled water. After that, the PVA solution was mixed with the centrifuged graphene suspension at a ratio of 3:2 (in mL) to form the precursor. The mixture was stirred using ultrasonic cleaner for about 1 h to give the precursor enough viscosity so that it could be easily used in forming a film. Lastly, a suitable amount of precursors were spread thinly on the glass substrate, and dried in an oven with a temperature of 56 °C to form the graphene-PVA film. The dispersion state of graphene flakes in the PVA matrix is detected by using field emission scanning electron microscopy (FESEM), and Fig. 1 shows a typical FESEM image of the cross-section of the graphene-PVA film with a ratio of 3:2. As observed, the graphene flakes are clearly well dispersed in the PVA matrix.

The thickness of the fabricated graphene-PVA film was around 50 μm and the insertion loss of the SA was measured at around 1.5 dB at 1550 nm. To construct the passive SA, a small piece of the fabricated film was sandwiched between two fiber ferrules. Then the SA was integrated into the laser cavity, with 3 m long Er-doped fiber (EDF) as a gain medium. It was pumped with a 1480 nm laser diode, coupled via a wavelength division multiplexer as shown in Fig. 2. The EDF used has absorptions of 15 and 26 dB/m at 980 and 1530 nm, respectively. An optical isolator ensures unidirectional light propagation. Polarization controller (PC) is used to optimize Q-switching and control the stability of the laser. A 20% port of an optical coupler provides the laser output. The Q-switching operation is evaluated by a 460 kHz bandwidth photodiode and an oscilloscope. An optical spectrum analyzer with a spectral resolution of 0.02 nm measures the output spectrum. The total cavity length of the ring resonator was measured to be around 9 m.

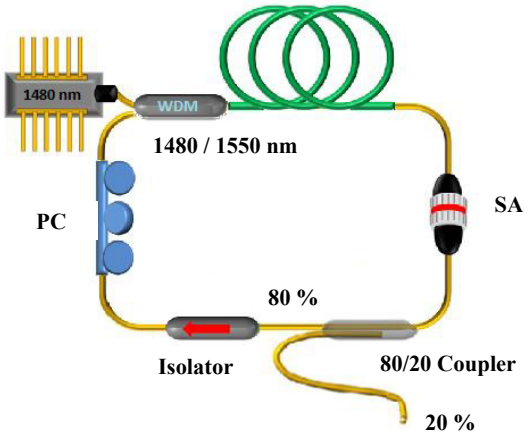

Fig. 2. Configuration of the Q-switched EDFL with graphene SA.

Raman spectroscopy was carried out to analyze the presence of graphene layer in the fabricated graphene-PVA film. Figure 3 shows the obtained Raman spectrum, which clearly indicates the three prominent peaks of D, G, and 2D bands at approximately 1341, 1603, and 2910 cm^{-1} respectively. The G band is an intrinsic feature of graphite layers and is related to the tangential vibration of sp^2 carbons, whereas the D band is associated with the vibrations of carbon atoms with sp^3 electronic configuration of disordered graphite. The 2D

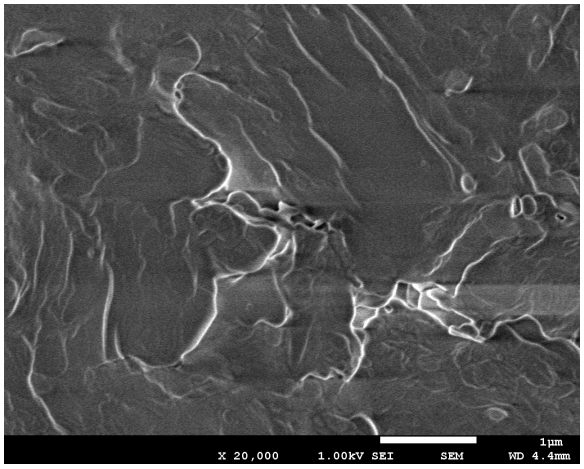

Fig. 1. FESEM image of graphene-PVA film.

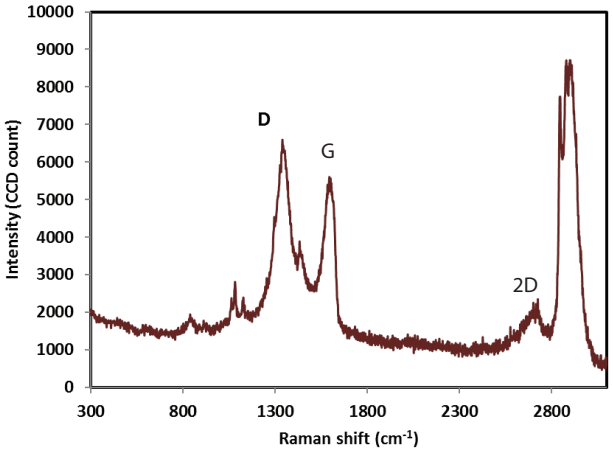

Fig. 3. Raman spectrum of the fabricated SA.

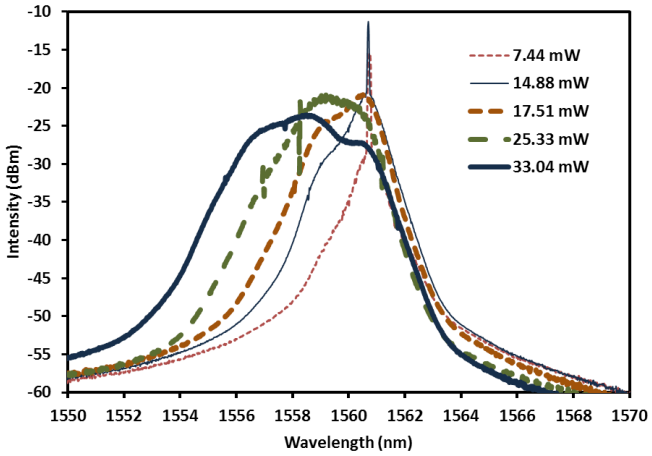

Fig. 4. Optical spectrum of Q-switched EDFL at various pump power ranging from 7.4 to 33.0 mW.

band always exists in grapheme but does not represent the defect in lattice. Although the intensity ratio of the D and G bands of the graphene sheets is about 1.2, defects are considered present in the graphene samples. However, the amount of structural defects is not significant because the D peak is not very broad[18]. The intensity ratio between G and 2D peak can be used to determine the number of graphene layer. Usually a single-layer graphene has a low-intensity ratio, usually less than 0.5 whereas, multi-layer graphene shows higher intensity ratio (≥ 1)[19]. The shape of the 2D peak can also be used to estimate the number of graphene layers. As shown in Fig. 3, we obtained a G/2D peak ratio of 0.6, which indicates that the graphene has a multi-layer structure. As the graphene layer increases, the full-width at half-maximum (FWHM) of the 2D peak follows[20]. As also shown in Fig. 3, the FWHM for G and 2D peaks are obtained at 50 and 104 cm^{-1}, respectively.

Stable and self-starting Q-switching operation is obtained just by adjusting the pump power over threshold of 7.4 mW. The repetition rate is pump dependent up to 33.0 mW, a typical signature of Q-switching. Figure 4 shows the output spectrum of the Q-switched laser at different pump powers ranging from 7.4 to 33.0 mW. As seen in Fig. 4, the laser starts to operate at 1560.7 nm before it is shifted to a shorter wavelength as the pump power increases. This is attributed to the Er gain which increases with the pump power and thus the operating wavelength shifts to a lower loss region. Pulse broadening is also observed with the increment of pump power due to the self-phase modulation effect. At the maximum pump power of 33 mW, the laser operates at a wavelength of 1558.5 nm with optical-to-signal noise ratio of more than 40 and 3 dB bandwidth of about 3.2 nm.

Figures 5(a) and (b) show the oscilloscope traces of the Q-switched pulse train at pump powers of 7.4 and 33.0 mW, respectively. Both pulse trains show typical

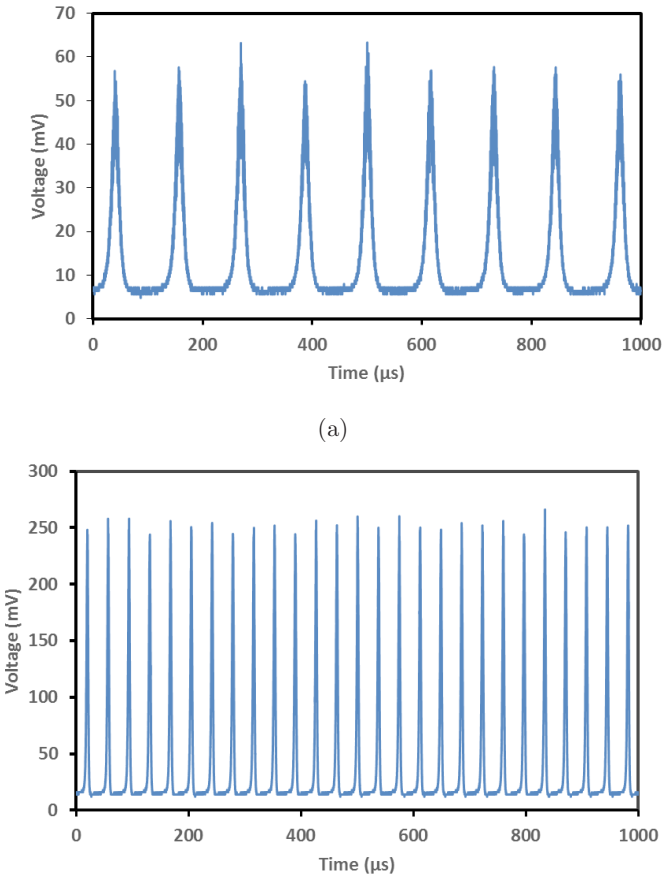

Fig. 5. Typical pulse trains from the Q-switching at two different pump powers: (a) 7.4 and (b) 33.0 mW.

features of passive Q-switching and are free from noticeable timing jitter. The pulse train has the period of 116 and 37 μs, which corresponds to repetition rates of 8.6 and 27.0 kHz at pump powers of 7.4 and 33.0 mW, respectively. Figures 6(a) and (b) show the corresponding pulse envelops, which have the symmetrical Gaussian-like shape with FWHMs of 18.56 and 3.56 μs, respectively. The pulse signal pedestal is not at zero voltage level in both Figs. 5 and 6 due to the detected noise level of the equipment.

In a passively Q-switched laser the cavity loss is modulated by the SA whose transmission/reflection depends on the light intensity. Basically, the pulse is released when the cavity energy reaches a certain value determined by the absorber saturation fluence. Therefore, unlike in mode-locked laser, where the repetition rate is fixed by the cavity length, in the Q-switched laser, the rate depends on the stored energy or pump power. Figure 7 shows the repetition rate and the pulse width against pump power. The repetition rate has a monotonically increasing, near-linear relationship with the pump power because the pulse generation relies on saturation. On the other hand, the pulse width is inversely proportional to the pump power, where the

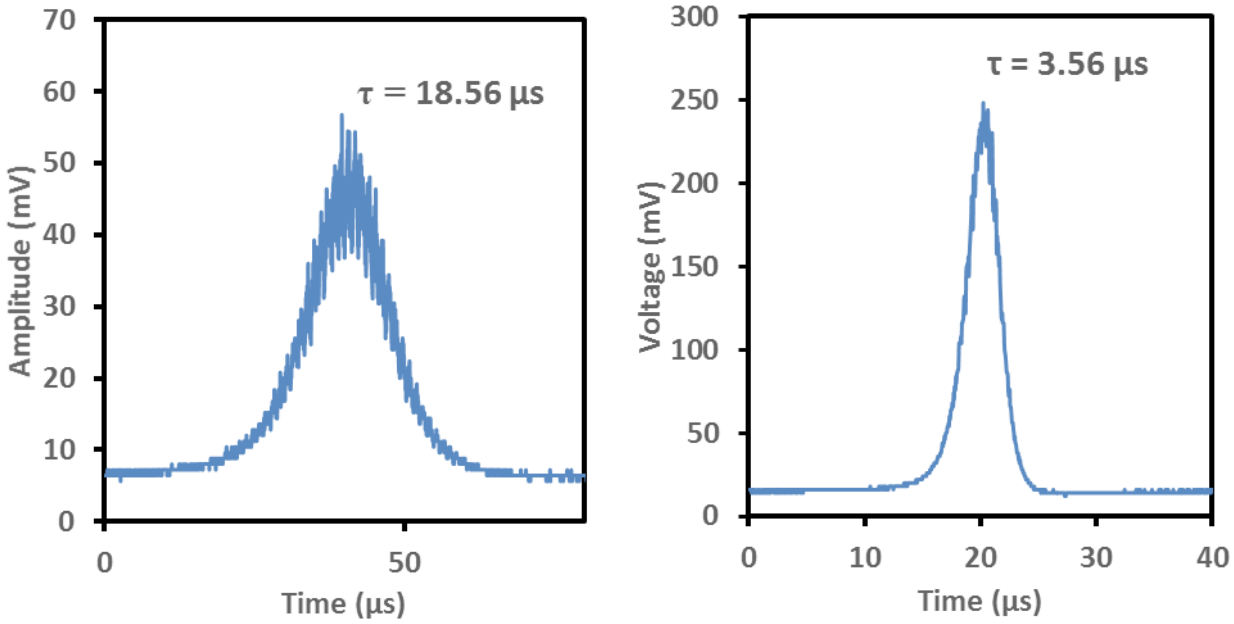

(a) (b)

Fig. 6. Typical single envelop of the Q-switching pulse at two different pump powers: (a) 7.4 mW and (b) 33.0 mW.

pulse duration becomes shorter as the pump power increases, as shown in Fig. 7. For instance, when the pump power is tuned from 7.4 to 33.0 mW, the pulse train repetition rate varies from 8.6 to 27.0 kHz whereas, the pulse width drops from 18.6 to 3.6 μs. The pulse width is expected to decrease further if the pump power can be augmented beyond 33.0 mW as long as it is still kept below the damage threshold of the graphene-based SA. The duration of long pulse is mainly relative to the long length of the cavity, which resulted in a relatively longer cavity lifetime[21]. Shortening the total cavity length of the fiber laser is another alternative to getting a shorter pulse.

As a comparison, the performance of the EDFL is also investigated with a graphene-PEO polymer film-based SA. The graphene-PEO film was prepared using the same process as the graphene PVA. Figure 8 shows the average output power and pulse energy against the pump power for both EDFLs configured with graphene PVA and graphene-PEO polymer composite film-based SA. It is clearly discerned that the threshold input pump power for graphene-PEO film-based SA is obtained at around 29 mW, which is higher than graphene-PVA film-based SA. With the graphene-PVA-based SA, both average power and energy show an increasing trend with the increase in the pump power up to 27.9 and 14.9 mW, respectively. Then, they start to saturate and decrease due to the increase in timing jitter noise in the cavity. The maximum pulse energy of 39.4 nJ was obtained at pump power of 14.9 mW. On the other hand, with the graphene-PEO-based SA, the average output power slightly increases with

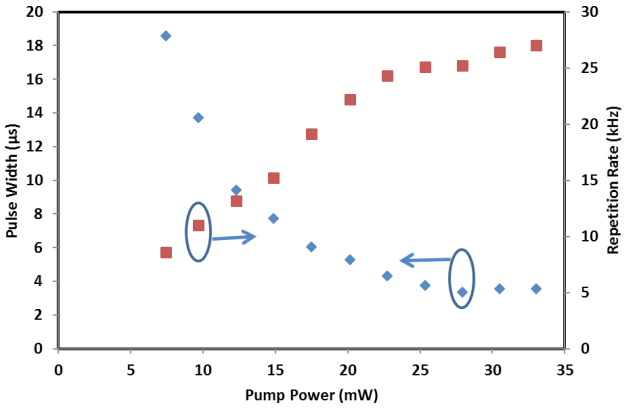

Fig. 7. Repetition rate and pulse width as a function of pump power.

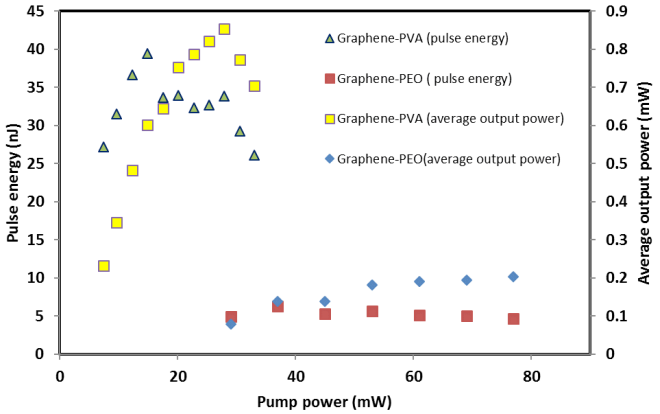

Fig. 8. Average output power and pulse energy as a function of pump power.

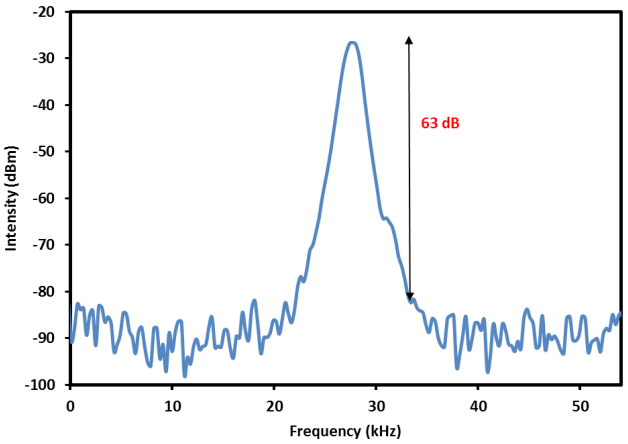

Fig. 9. RF spectrum of the output pulse train obtained with graphene PVA.

the pump while maintaining the pulse energy at around 5 nJ. This shows that the graphene PVA outperformed the graphene PEO SA in terms of attainable output power and energy. This is probably due to the graphene flakes, which are better dispersed in the PVA compared with the PEO matrix. The pulse energy could be further improved by reducing the insertion loss of the graphene SA and optimizing the laser cavity.

The radio frequency (RF) measurement of the output pulse intensity at pump power of 33.0 mW is shown in Fig. 9 for the proposed EDFL with graphene PVA SA. The peak-to-pedestal extinction is about 63 dB, confirming pulse stability. It is possible to operate the proposed Q-switched EDFL at a very low pump power which can also be achieved by using a cheap laser diode. Thus, this laser has a great potential to be developed as low-cost light source. Such low-threshold Q-switched EDFL could provide a simple, low cost and convenient light source for metrology, environmental sensing, and biomedical diagnostics.

In conclusion, we experimentally demonstrate a simple and low-cost Q-switched EDFL using a graphene-PVA film-based SA. The graphene suspension is produced by electrochemical exfoliation process and mixed with PVA solution as the host polymer to produce a thin film. A small portion of the film is inserted between two ferrules to form a SA which acts as a passive Q-switcher in the EDFL ring cavity. We obtain a pulse train operating at the 1560 nm region with a repetition rate that vary from 8.6 to 27 kHz as the pump power is increased from the threshold pump power of 7.4 to 33.0 mW. The minimum pulse width of 3.56 μs is obtained at the maximum pump power of 33.0 mW, whereas the maximum pulse energy of 39.4 nJ is obtained at a pump power of 14.9 mW. We believe that a higher performance Q-switched EDFL is achievable with the optimization of the graphene SA and laser cavity.

This work was financially supported by the Ministry of Education and the University of Malaya under Grant Nos. ER012-2013A and RP008D-13AET.

References

1. B. Q. Yao, X. Yu, X. L. Liu, X. M. Duan, Y. L. Ju, and Y. Z. Wang, Chin. Phys. Lett. **30,** 034207 (2013).
2. Y. X. Fan, F. Y. Lu, S. L. Hu, K. C. Lu, H. J. Wang, X. Y. Dong, J. L. He, and H. T. Wang, Opt. Lett. **29,** 724 (2004).
3. Y. Wang and C. Q. Xu, Appl. Opt. **45,** 2058 (2006).
4. R. Su, P. Zhou, X. Wang, R. Tao, and X. Xu, High Power Laser Sci. Eng. **2,** e3 (2014).
5. J. Jabczynski, W. Zendzian, and J. Kwiatkowski, Opt. Express **14,** 2184 (2006).
6. J. H. Lin, H. R. Chen, H. H. Hsu, M. D. Wei, K. H. Lin, and W. F. Hsieh, Opt. Express **16,** 16538 (2008).
7. O. Okhotnikov, A. Grudinin, and M. Pessa, New J. Phys. **6177,** 1 (2004).
8. S. W. Harun, M. A. Ismail, F. Ahmad, M. F. Ismail, R. M. Nor, N. R. Zulkepely, and H. Ahmad, Chin. Phys. Lett. **29,** 114202 (2012).
9. N. Kasim, A. H. H. Al-Masoodi, F. Ahmad, Y. Munajat, H. Ahmad, and S. W. Harun, Chin. Opt. Lett. **12,** 031403 (2014).
10. Z. Yu, Y. Song, C. Tian, J. Li, X. Zhang, and Y. Wang, Proc. SPIE **8551,** 855115 (2012).
11. C. L. Anyi, N. M. Ali, A. A. Rahman, S. W. Harun, and H. Arof, Ukr. J. Phys. Opt. **14,** 212 (2013).
12. H. F. Ma, Y. G. Wang, W. Zhou, J. Y. Long, D. Y. Shen, and Y. S. Wang, Laser Phys. **23,** 035109 (2013).
13. F. Bonaccorso, Z. Sun, T. Hasan, and A. C. Ferrari, Nat. Photon. **4,** 611 (2010).
14. S. Han, X. Li, H. Xu, Y. Zhao, H. Yu, H. Zhang, Y. Wu, Z. Wang, X. Hao, and X. Xu, Chin. Opt. Lett. **12,** 011401 (2014).
15. L. M. Zhao, D. Y. Tang, H. Zhang, X. Wu, Q. Bao, and K. P. Loh, Opt. Lett. **35,** 3622 (2010).
16. G. Sobon, J. Sotor, I. Pasternak, A. Krajewska, W. Strupinski, and K. M. Abramski, Opt. Express **21,** 12797 (2013).
17. P. L. Huang, S. C. Lin, C. Y. Yeh, H. H. Kuo, S. H. Huang, G. R. Lin, L. J. Li, C. Y. Su, and W. H. Cheng, Opt. Express **20,** 2460 (2012).
18. Z. Sun, T. Hasan, F. Torrisi, D. Popa, G. Privitera, F. Wang, F. Bonaccorso, D. M. Basko, and A. C. Ferrari, ACS Nano. **4,** 803 (2010).
19. S. Chen, L. Brown, M. Levendorf, W. Cai, S. Y. Ju, J. Edgeworth, X. Li, C. W. Magnuson, A. Velamakanni, R. D. Piner, J. Kang, J. Park, and R. S. Ruoff, ACS Nano. **5,** 1321 (2011).
20. A. C. Ferrari, J. C. Meyer, V. Scardaci, C. Casiraghi, M. Lazzeri, F. Mauri, S. Piscanec, D. Jiang, K. S. Novoselov, S. Roth, and A. K. Geim, Phys. Rev. Lett. **97,** 187401 (2006).
21. L. Zhang, J. T. Fan, J. H. Wang, J. M. Hu, M. Lotya, G. Z. Wang, and Y. Feng, Laser Phys. Lett. **9,** 888 (2012).